INTERNATIONAL JOURNAL OF COMPUTER MATHEMATICS, 2018
VOL. 95, NOS. 6–7, 1423–1443
https://doi.org/10.1080/00207160.2018.1437911

Taylor & Francis
Taylor & Francis Group

On the numerical solution and dynamical laws of nonlinear fractional Schrödinger/Gross–Pitaevskii equations

Xavier Antoine [a], Qinglin Tang [b,c] and Jiwei Zhang [d]

[a]Institut Elie Cartan de Lorraine, UMR CNRS 7502, Université de Lorraine, Vandoeuvre-lès-Nancy Cedex, France; [b]Department of Mathematics, Sichuan University, Chengdu, China; [c]The Institute of Mathematical Sciences, Chinese University of Hong Kong, Hong Kong; [d]Beijing Computational Science Research Center, Beijing, China

ABSTRACT

The purpose of this paper is to discuss some recent developments concerning the numerical simulation of space and time fractional Schrödinger and Gross–Pitaevskii equations. In particular, we address some questions related to the discretization of the models (order of accuracy and fast implementation) and clarify some of their dynamical properties. Some numerical simulations illustrate these points.

ARTICLE HISTORY
Received 13 May 2017
Revised 11 September 2017
Accepted 16 September 2017

KEYWORDS
Fractional Schrödinger equation; fractional Gross–Pitaevskii equations; dynamical laws; conservation properties; discretization schemes; accuracy order; fast implementation

2010 AMS SUBJECT CLASSIFICATIONS
35Q41; 34A08; 65M06; 65M70

1. Introduction

The development of fractional partial differential equations (PDEs) has grown impressively during the last few years, because of the huge potential of emerging applications in science. In particular, some important impacts concern fractional quantum dynamics based on the space or/and time Fractional Schrödinger equation and its nonlinear version (SFNLSE or TFNLSE) [1,13,23,28,30,32,33,57,63,65,78]. The fractional nonlinear Schrödinger equation is used to describe the nonlocal phenomena in quantum physics and to explore the quantum behaviours of either long-range interactions or time-dependent processes with many scales [1,44,45,47–49,57,63,73,80,81]. For example, FNLSE arise in the modelling of quantum fluids of light [28], boson stars [13,32,33] and polariton condensates [65]. Some analytical and approximate solutions have been considered, e.g. for the TFSE [43,64]. The complexity of FNLSE with different potentials and nonlinearities requires the development of efficient and accurate numerical simulations [24,31,34,36,42,44,53,54,61,79] to go further.

The aim of the paper is not to review and compare all the numerical methods that have been designed during the last years for the SFNLSE and TFNLSE but rather to discuss some developments of efficient, accurate, stable and physically relevant numerical schemes through examples, most particularly regarding the dynamical laws for FNLSE where many questions remain open. For the integer-order NLSE, the picture is now pretty clear [7,12] and the development of high-order schemes

CONTACT Xavier Antoine xavier.antoine@univ-lorraine.fr Institut Elie Cartan de Lorraine, UMR CNRS 7502, Université de Lorraine, Inria Nancy-Grand Est, SPHINX Team, F-54506 Vandoeuvre-lès-Nancy Cedex, France

follow a well-defined route, in particular concerning the discrete dynamical laws that a numerical scheme should mimic regarding the continuous physical equations. Concerning the Gross–Pitaevskii equation (GPE) arising in Bose–Einstein Condensation (BEC) [66] as a generalization of the NLSE, numerous extensions to relevant physical situations are now clarified [4,7,12] (multi-components, nonlocal nonlinear interactions, etc.). For the fractional case, the situation is more complicated and still needs to be analysed deeply. The aim of this paper is to contribute to the topic, by discussing the question of the dynamical laws that the space or time fractional NLSE/GPE should fulfil to yield correct physical solutions, while being efficient, accurate and stable. The schemes used here have mainly been designed by the authors and serve as examples to illustrate the purpose. Finally, the paper can be seen as a complement of Antoine *et al.* [7] while being much more prospective and does not pretend to be a review paper.

The plan of the paper is the following. In Section 2, we recall the main results concerning the features of the most popular schemes for the standard NLSE/GPE. In Section 3, we develop the space fractional NLSE/GPE, some of its properties, the numerical schemes leading to a fast implementation with coherent physical features, and finally provide some numerical examples. In Section 4, we consider the TFNLSE and discuss the dynamical laws. This case is the most difficult to analyse since only a few theoretical results are available. Then, we explain some fast evaluation schemes for the TFNLSE and report some illustrative examples to address the difficult issue of the dynamical laws that can be expected at the discrete level, according to the underlying fractional equation. We finally end the paper with a conclusion and draw a few perspectives in Section 5.

2. The standard NLSE/GPE

2.1. Integer-order models and dynamical properties

We start by considering the following time-dependent cubic NLSE [12,71]

$$\mathrm{i}\partial_t \psi(t,\mathbf{x}) = \left[-\tfrac{1}{2}\Delta + V(\mathbf{x}) + \beta|\psi(t,\mathbf{x})|^2\right]\psi(t,\mathbf{x}), \quad \mathbf{x}\in\mathbb{R}^d, \quad t>0, \tag{1}$$

$$\psi(t=0,\mathbf{x}) = \psi_0(\mathbf{x}), \quad \mathbf{x}\in\mathbb{R}^d. \tag{2}$$

In the above equations, $i=\sqrt{-1}$ is the complex unit, t is the time variable, $\mathbf{x}\in\mathbb{R}^d$ is the spatial variable (for $d=1,2,3$), $\psi := \psi(t,\mathbf{x})$ is the unknown complex-valued wave function, $\Delta = \nabla^2$ is the usual Laplace operator in dimension d (and ∇ the gradient operator) and $\psi_0 := \psi_0(\mathbf{x})$ is a given complex-valued initial data. The real-valued external potential function $V := V(\mathbf{x})$ is given and its definition is related to the underlying application. For instance, for BEC, it can be chosen as a harmonic confining trap, an optical lattice potential or even a quadratic-plus-quartic function [37,38,66]; for nonlinear optics applications, it could be set as an attractive potential. The potential function V may also depend on the time variable t or can even be stochastic. The standard cubic nonlinearity involves the density function $\rho := |\psi|^2 := \psi\bar{\psi}$, the parameter β being the nonlinearity strength [12,66] (positive for a repulsive/defocusing interaction and negative for an attractive/focusing interaction) and $\bar{\psi}$ the complex conjugate of the wave function ψ. Other local nonlinearities are used in nonlinear optics, i.e. cubic-quintic nonlinearity or saturation of the intensity nonlinearity [7,18], or even nonlocal nonlinearities like for dipolar gazes [17]. The cubic NLSE (1) is also called the GPE in the framework of BEC [4,66].

Important dynamical properties are verified for the solution ψ of Equation (1). Here, we mention the most important ones that are also hopefully expected to be fulfilled at the discrete level to get some robust numerical methods. The integer-order NLSE (1) is a dispersive PDE that is time reversible, i.e. it is unchanged under the change of time variable $t\to -t$, and next taking the conjugate into the equation. A second crucial property is gauge invariance, that is, if $V\to V+C$ ($C\in\mathbb{R}$), then the solution $\psi\to\psi\,\mathrm{e}^{-iCt}$ implies that the density $\rho=|\psi|^2$ is unchanged. The NLSE (1) conserves some

quantities over the time, such as the mass and energy [12,29,71], for $t \geq 0$,

$$\mathcal{N}(t) := \|\psi(t,\cdot)\|_2^2 = \int_{\mathbb{R}^d} |\psi(t,\mathbf{x})|^2 \,\mathrm{d}\mathbf{x} \equiv \int_{\mathbb{R}^d} |\psi(0,\mathbf{x})|^2 \,\mathrm{d}\mathbf{x} := \mathcal{N}(0), \tag{3}$$

$$\mathcal{E}_2(t) := \int_{\mathbb{R}^d} \left[\frac{1}{2}|\nabla\psi(t,\mathbf{x})|^2 + V(\mathbf{x})|\psi(t,\mathbf{x})|^2 + \frac{\beta}{2}|\psi(t,\mathbf{x})|^4 \right] \mathrm{d}\mathbf{x} \equiv \mathcal{E}_2(0). \tag{4}$$

In the free-potential situation, i.e. $V(\mathbf{x}) \equiv 0$, the momentum and angular momentum are conserved [71]. The NLSE (1) admits the plane wave solution as $\psi(t,\mathbf{x}) = A\,\mathrm{e}^{\mathrm{i}(\mathbf{k}\cdot\mathbf{x}-\omega t)}$, where the time frequency ω, amplitude A and spatial wave number $\mathbf{k}$ satisfy the dispersion relation

$$\omega = \frac{|\mathbf{k}|^2}{2} + \beta|A|^2. \tag{5}$$

More dynamical properties of the NLSE (1) such as the well-posedness and finite time blow-up and the properties of its solitary solutions in 1d can be found in [7,12,18,29,71] and references therein.

2.2. Overview of popular numerical schemes

To numerically simulate the dynamical system (1), the full-space problem usually is truncated suitably so that the perturbation of the solution at the boundary is negligible. This results therefore in an initial boundary-value problem. In this paper, we restrict ourselves to consider the case where the solution is confined within domain $\mathcal{D} :=]a;b[^d$. This is a standard situation, particularly for BEC, where the potential is strongly confining. Therefore, the choice of the boundary condition (BC) does not essentially modify the solution if $\mathcal{D}$ is large enough. The specific BCs are chosen according to the spatial discretization scheme one uses. More precisely, when a second-order finite-difference (FD) scheme is applied (see Section 4.2), we impose a homogeneous Dirichlet BC. For the Fourier pseudospectral (SP) scheme (see Section 3.2), we will use a periodic BC. In addition, if the solution ψ is not confined in $\mathcal{D}$, i.e. ψ can strike the boundary, then much more complicated BCs are required, such as the transparent, artificial and absorbing BCs as well as perfectly matched layers (see references [6,11,85] for the integer-order Schrödinger equations and [83] for fractional order problems). However, this is out of the scope of the current paper.

Considering now the time approximation schemes for the Schrödinger equation, it is well known that building schemes that preserve at the discrete level the physical properties discussed above in Section 2.1 is nontrivial. We do not develop here a full discussion and rather choose to report in Table 1 the conclusion from [7] for four specific schemes (where the discretization of the physical quantities must be suitably defined thanks to the approximation scheme). TSSP (respectively TSFD) refers to the second-order Strang time-splitting scheme with SP [15,16,21,59] (respectively second-order FD) approximation in space. CNFD and ReFD are related to the second-order Crank–Nicolson (CN) and relaxation schemes [20] with FD.

Let us now discuss the convergence properties of the various schemes as well as some of the implementation issues, taking the one-dimensional case to explain the technical details. We assume here that we discretize in space with $J-1$ equally spaced interior points, i.e. $x_j = jh_x, 0 \leq j \leq J$ (with $x_0 = a$ and $x_J = b$) in $]a;b[$ (the extension to the d-dimensional situation is direct). The spatial mesh size is then $h = h_x = (b-a)/J$. In practice, we wish to compute the numerical solution from $t = 0$ to a maximal computational time $t = T$. Let us introduce the $N+1$ uniformly distributed discrete times $(t_n)_{0\leq n\leq N}$ such that: $t_n = n\Delta t$, for $n = 0,\ldots,N$, with $\Delta t := T/N$. The four schemes are unconditionally stable, i.e. there is no Courant–Friedrichs–Lewy (CFL) condition involving h and Δt. In addition, the schemes are all second-order in time, and in space second-order for FD or spectral for SP.

The only fully explicit scheme is TSSP, where the nonlinearity and potential terms can be directly integrated in time, leading then to diagonalize the remaining free-space linear Schrödinger opera-

Table 1. Integer-order NLSE: physical/numerical properties of various numerical methods in the d-dimensional case.

Method	TSSP	CNFD	ReFD	TSFD
Time reversible	Yes	Yes	Yes	Yes
Time transverse invariant	Yes	No	No	Yes
Mass conservation	Yes	Yes	Yes	Yes
Energy conservation	No	Yes	Yes[a]	No
Dispersion relation	Yes	No	No	Yes
Unconditional stability	Yes	Yes	Yes	Yes
Time accuracy	2nd	2nd	2nd	2nd
Spatial accuracy	Spectral	2nd	2nd	2nd
Explicit scheme	Yes	No	No	No
Memory storage at t_n	$\mathcal{O}(J^d)$	$\mathcal{O}(J^d)$	$\mathcal{O}(J^d)$	$\mathcal{O}(J^d)$
Computational cost	$\mathcal{O}(J^d \log J)$	$\gg \mathcal{O}(J^d)$[b]	$\mathcal{O}(J^d \log J)$[c]	$\mathcal{O}(J^d \log J)$[d]

[a] Only for cubic nonlinearity.
[b] Depends on the nonlinear solver.
[c] if $d = 1$, $\mathcal{O}(J)$.
[d] if $d = 1$, $\mathcal{O}(J)$.

tor through the FFT (see also Section 3.2) at a computational cost $\mathcal{O}(J^d \log J)$. In terms of memory storage, we need the values of the solution $(\psi_j^n)_{0\le j\le J}$ (with $\psi_j^n \approx \psi(x_j, t_n)$, and $\psi^n \approx \psi(\cdot, t_n)$) only at time t_n since no time memory effect is involved into the equation (indeed, $\mathrm{i}\partial_t$ is a local operator). TSFD and ReFD are linearly implicit schemes since the nonlinearity is made explicit. Hence, each time step requires to store and solve the associated linear system, i.e. corresponding to $\mathcal{O}(J^d)$ coefficients to store and to $\mathcal{O}(J^d \log J)$ operations with an adapted fast linear algebra solver for structured systems. Of course, the solution must also be stored at time t_n. Finally, since the CNFD scheme is fully implicit, each time step requires the solution to a nonlinear system that solved by iterative methods. As a consequence, the computational cost is clearly much larger than $\mathcal{O}(J^d)$, while the memory storage remains $\mathcal{O}(J^d)$. Table 1 resumes the main properties.

Let us remark that high-order TSSP schemes [14,69,75] can also be built for the NLSE/GPE. Nevertheless, these approaches do not always apply for some equations, e.g. when the system is non-autonomous. Recent high-order schemes (exponential integrators [22,74,76], IMEXSP [8], etc.) with time-stepping techniques have been designed to get new efficient solvers that could be combined with SP approximation schemes. We also note that ReFD can be extended to include the SP approximation, resulting in the ReSP scheme given in [5]. When developing the ReSP method, each time step t_n requires the solution to a n-dependent linear system that can be easily solved by combining an iterative Krylov subspace solver (GMRES) and an adapted preconditioner. From the analysis above, we see that TSSP provides a suitable way to solve the NLSE.

3. The space FNLSE/FGPE

3.1. Space fractional models and dynamical properties

We consider now the specific Space Fractional NLSE (SFNLSE)

$$\mathrm{i}\partial_t \psi(t,\mathbf{x}) = \left[\tfrac{1}{2}(-\Delta)^s + V(\mathbf{x}) + \beta|\psi(t,\mathbf{x})|^2\right]\psi(t,\mathbf{x}). \tag{6}$$

This equation is called SFGPE in the framework of the GPE for BECs. The real-valued parameter $s > 0$ is the space fractional order defining the nonlocal dispersive interaction. The fractional dispersion is called *superdispersion* (respectively *subdispersion*) for $s > 1$ (respectively $s < 1$) [9]. The fractional kinetic operator is defined via a Fourier integral operator

$$(-\Delta)^s \psi = \frac{1}{(2\pi)^d}\int_{\mathbb{R}^d} \hat{\psi}(\mathbf{k})|\mathbf{k}|^{2s}\,\mathrm{e}^{\mathrm{i}\mathbf{k}\cdot\mathbf{x}}\,\mathrm{d}\mathbf{k}, \tag{7}$$

where the Fourier transform is

$$\hat{\psi}(\mathbf{k}) = \int_{\mathbb{R}^d} \psi(\mathbf{x})\, \mathrm{e}^{-\mathrm{i}\mathbf{k}\cdot\mathbf{x}}\, \mathrm{d}\mathbf{x}.$$

For $s=1$, the SFNLSE (6) simplifies to the standard cubic NLSE (1). A more general form of Equation (6) can be found in [9] where a nonlocal nonlinear interaction term given by a convolution kernel $\mathcal{U}$ (corresponding to a Coulomb or dipolar interaction) is added to the cubic nonlinearity, the Laplace operator involves a mass term m and finally a rotation term $-\Omega L_z\psi$ (where $L_z = -\mathrm{i}(x\partial_y - y\partial_x)$ is the z-component of the angular momentum, Ω representing the rotating frequency) is included into the equation. More precisely, the system writes (with $\lambda \in \mathbb{R}$)

$$\mathrm{i}\partial_t\psi(t,\mathbf{x}) = \left[\tfrac{1}{2}\left(-\Delta + m^2\right)^s + V(\mathbf{x}) + \beta|\psi|^2 + \lambda\Phi(t,\mathbf{x}) - \Omega L_z\right]\psi(t,\mathbf{x}), \tag{8}$$

$$\Phi(t,\mathbf{x}) = \mathcal{U} * |\psi(t,\mathbf{x})|^2, \quad \mathbf{x}\in\mathbb{R}^d, \quad t>0, \quad d\geq 2. \tag{9}$$

For Equations (6) and (8)–(9), the mass conservation $\mathcal{N}$ given by Equation (3) still holds. We can also define the conservation of a fractional energy $\mathcal{E}_s$ as follows:

$$\mathcal{E}_s(t) = \int_{\mathbb{R}^d}\left[\frac{1}{2}\bar{\psi}\left(-\nabla^2 + m^2\right)^s\psi + V|\psi|^2 + \frac{\beta}{2}|\psi|^4 + \frac{\lambda}{2}\Phi|\psi|^2 - \Omega\bar{\psi}L_z\psi\right]\mathrm{d}\mathbf{x} \equiv \mathcal{E}_s(0). \tag{10}$$

We remark that $m=0$ and the terms λ and Ω in Equation (10) shall be omitted if $d=1$. The equation is clearly still *time reversible and gauge invariant*. In addition, the dispersion relation (for $V=0$) now reads as follows:

$$\omega = \frac{|\mathbf{k}|^{2s}}{2} + \beta|A|^2. \tag{11}$$

In the case of Equations (8)–(9), extensions of some standard dynamical laws (mainly related to the angular momentum expectation and center of mass) have been stated in [9] for some values of s. Nevertheless, some questions still remain open such as the dynamical laws of the center of mass (for $s>1$) and condensate widths, the well-posedness of the SFNLSE with general s and attractive interaction (i.e. $\beta<0$).

3.2. Numerical schemes and their efficient implementation

From the conclusion of Section 2.2, a natural scheme for solving Equation (6) is to use an adapted TSSP scheme since the space fractional operator $(-\Delta)^s$ is naturally represented through an inverse Fourier transform as a pseudodifferential operator. Since the physics is confined within a finite computational domain, then periodic BCs can be set on the boundary. From $t=t_n$ to $t=t_{n+1}:=t_n+\Delta t$ and for the one-dimensional case ($d=1$, the extension being direct to $d\geq 2$), we solve the system in two steps. First, one considers

$$\mathrm{i}\partial_t\psi(t,x) = \left[V(x) + \beta|\psi|^2\right]\psi(t,x), \quad x\in]a;b[, \quad t_n\leq t\leq t_{n+1}, \tag{12}$$

for a time step Δt, and next we solve

$$\mathrm{i}\partial_t\psi(t,x) = \tfrac{1}{2}(-\partial_{xx})^s\psi(t,x), \quad x\in]a;b[, \quad t_n\leq t\leq t_{n+1}, \tag{13}$$

with periodic BCs at $\{a;b\}$ for the same time step. The linear subproblem (13) is discretized in space by the Fourier SP method and integrated in time exactly in the Fourier space. Similarly to $s=1$,

the nonlinear subproblem (12) preserves the density, i.e. $|\psi(t,x)|^2 \equiv |\psi(t=t_n,x)|^2 = |\psi^n(x)|^2$, leading to

$$\psi(t,x) = \mathrm{e}^{-\mathrm{i}\left[V(x)+\beta|\psi^n(x)|^2\right](t-t_n)}\psi^n(x), \quad x \in]a;b[, \quad t_n \le t \le t_{n+1}. \tag{14}$$

Let us introduce J as an even positive integer and $\mu_\ell = 2\pi\ell/(b-a)$, for $-\frac{J}{2} \le \ell \le \frac{J}{2}-1$. We denote by $\boldsymbol{\psi}^n$ the numerical solution at time $t=t_n$, with components ψ_j^n, $0 \le j \le J$, for the initial data $\boldsymbol{\psi}^0 = (\psi_0(x_j))_{0\le j\le J}$. A second-order TSSP scheme for solving Equation (6) is

$$\psi_j^{(1)} = \sum_{\ell=-J/2}^{J/2-1} \mathrm{e}^{-\mathrm{i}\Delta t/4|\mu_\ell|^{2s}}(\widehat{\boldsymbol{\psi}^n})_\ell \, \mathrm{e}^{\mathrm{i}\mu_\ell(x_j-a)}, \tag{15}$$

$$\psi_j^{(2)} = \psi_j^{(1)} \, \mathrm{e}^{-\mathrm{i}\Delta t\left[V(x_j)+\beta|\psi_j^{(1)}|^2\right]}, \tag{16}$$

$$\psi_j^{n+1} = \sum_{\ell=-J/2}^{J/2-1} \mathrm{e}^{-\mathrm{i}\Delta t/4|\mu_\ell|^{2s}}\widehat{(\boldsymbol{\psi}^{(2)})}_\ell \, \mathrm{e}^{\mathrm{i}\mu_\ell(x_j-a)}, \tag{17}$$

for $0 \le j \le J$ and $n \ge 0$. Here, $(\widehat{\boldsymbol{\psi}^n})_\ell$ and $\widehat{(\boldsymbol{\psi}^{(2)})}_\ell$ are the discrete Fourier series coefficients of $\boldsymbol{\psi}^n$ and $\boldsymbol{\psi}^{(2)}$, respectively. The TSSP scheme (15)–(17) for s inherits of the properties for $s=1$ given in Table 1 and can be extended to high-order time-splitting schemes.

The extension to the general system (8)–(9) is developed in [9]. It essentially needs to take care about the efficient spectral approximation of the nonlocal nonlinear interaction term (based on a Gaussian-Sum evaluation) and the elimination of the rotating term through a rotating Lagrangian coordinates transformation. This latter modification results in the appearance of a new time-dependent potential which must be integrated numerically in the TSSP scheme. Let us finally remark that ReSP could also be extended to the SFNLSE, and that, more generally, any well-designed high-order time integrator (TSSP, IMEXSP, etc.) could be applied here.

3.3. Numerical examples

In this section, we consider the effect of the fractional order s on the dynamics of the SFNLSE for various situations. We only show the results in 1d and 2d. For $d=1,2$, the potential, computational domain and time step are chosen as follows:

$$V(\mathbf{x}) = \frac{1}{2}\begin{cases} \gamma_x^2 x^2, & d=1, \\ \gamma_x^2 x^2 + \gamma_y^2 y^2, & d=2, \end{cases} \quad \mathcal{D} = \left]-\frac{64}{d}, \frac{64}{d}\right[^d, \quad \Delta t = 10^{d-5}. \tag{18}$$

Moreover, we take the mesh size h and initial data ψ_0 as follows:

$$\begin{aligned} &h = h_x = \tfrac{1}{64}, \quad d=1, \\ &h = h_x = h_y = \tfrac{1}{16}, \quad d=2, \end{aligned} \qquad \psi_0(\mathbf{x}) = \phi_{\mathrm{gs}}^{s_0}(\mathbf{x}-\mathbf{x}_0), \tag{19}$$

where $\phi_{\mathrm{gs}}^{s_0}$ is the ground states (gs) of the SFNLSE (6) (if $d=1$) and/or Equation (8) (with $m=\lambda=0$, if $d=2$) with potential given by $V(\mathbf{x})$ Equation (18) and fractional order s_0. The ground states

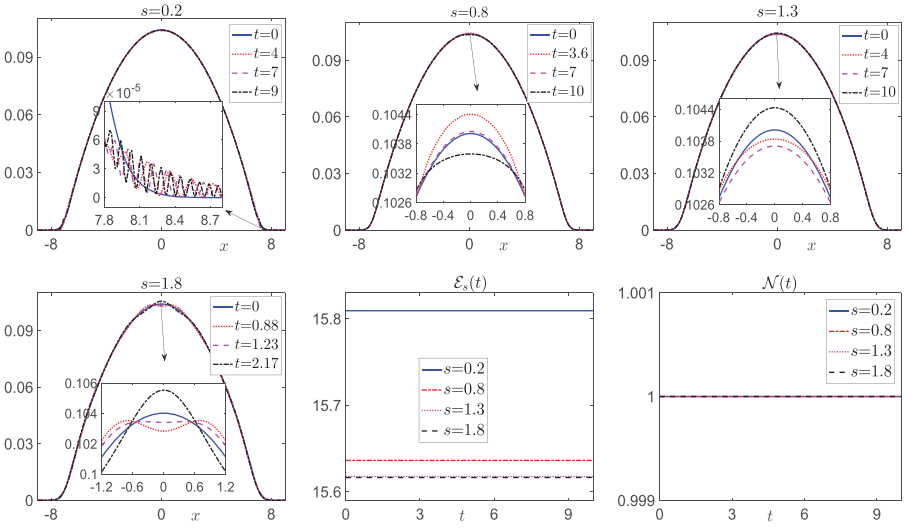

Figure 1. Density $|\psi(x,t)|^2$ at different times t and evolution of the mass $\mathcal{N}(t)$ and energy $\mathcal{E}_s(t)$ for different values of the fractional powers s for *Case 1* in Example 3.1.

can be computed either by the popular *gradient flow* method [9,12,13,19] or the recently developed *conjugated gradient flow* approach [10]. Here, we apply the method proposed in [9].

Example 3.1: Here, we consider a simple 1d case to show the difference of dynamics for various fractional powers s. For $d = 1$, we take $\gamma_x = 1$ in Equation (18) and $\beta = 250$ in Equation (6). We consider two cases of initial data $\psi_0(x)$ (see Equation (19)):

Case 1. Fix $s_0 = 1$ and $x_0 = 0$, i.e. always take the initial data as the ground states of classical NLSE, then only vary s.

Case 2. Take $s_0 = s$, and $x_0 = 8$, i.e. we take the initial data as the ground states of the SFNLSE with initial center shifted to x_0. Then, we consider the dynamics for different fractional orders s.

All the ground states are computed by using the preconditioned nonlinear conjugate gradient method developed in [10], eventually adapted to the SFNLSE. Figures 1 and 2 show the evolution of the density $|\psi|^2$, the mass $\mathcal{N}(t)$ and the energy $\mathcal{E}_s(t)$ for different fractional orders s in *Cases 1* and *2*. From these experiments and others not shown here for brevity, we could see that: (1) The mass and energy are conserved very well during the dynamics, for all the cases; (2) The fractional order s affects the dynamics of the density $|\psi|^2$ significantly and qualitatively (cf. Figure 1). Oscillations usually arise during the dynamics, and would sometimes turn to a chaotic dynamics for long-time simulations; (3) When s is larger, one needs larger domain sizes to well-resolved the solution in phase space, while a smaller mesh size h is needed if s is smaller; (4) For a center-shifted initial profile, the larger s is, the faster the center of mass oscillates (cf. Figure 2). Again, for a larger s, oscillation of the density occurs and chaotic dynamics arises (cf. Figure 2 for $s = 1.4$).

Example 3.2: Here, we investigate the dynamics of vortex lattice and vortex ring under different setups in 2d. To this end, the trapping potential $V(\mathbf{x})$ for preparing the ground states $\phi_{\rm gs}^{s_0}$ is chosen as Equation (18) with $\gamma_x = \gamma_y = 1$. We consider two types of ground states $\phi_{\rm gs}^{s_0}(\mathbf{x})$, i.e. the *Type 1* ground states of the SFNLSE (8) with parameters $s_0 = 1$, $\beta = 500$, $\Omega = 0.95$ and the *Type 2* with parameters $s_0 = 1.2$, $\beta = 100$, $\Omega = 1.7$.

Figure 3 (i) and (ii) shows the contour plot of the density $|\phi_{gs}^{s_0}|^2$ of these two types of ground states. Then, we consider the following six cases:

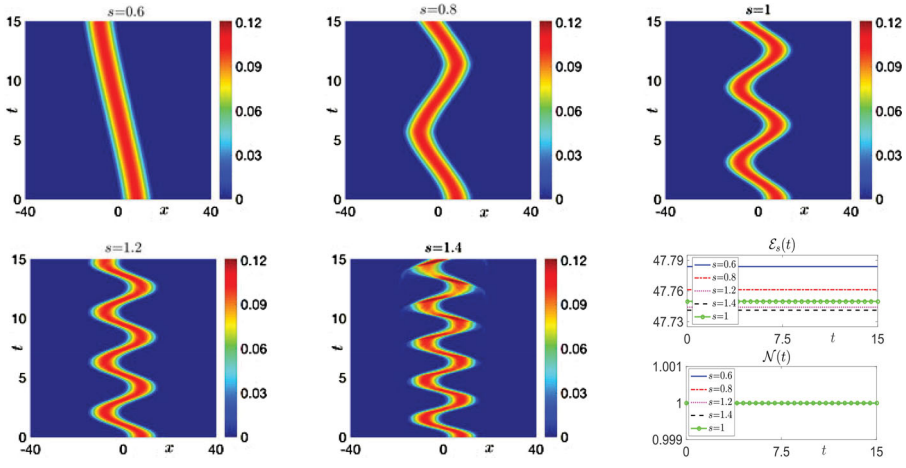

Figure 2. Evolution of the density $|\psi(x,t)|^2$, mass $\mathcal{N}(t)$ and energy $\mathcal{E}_s(t)$ for different fractional powers s for *Case 2* in Example 3.1.

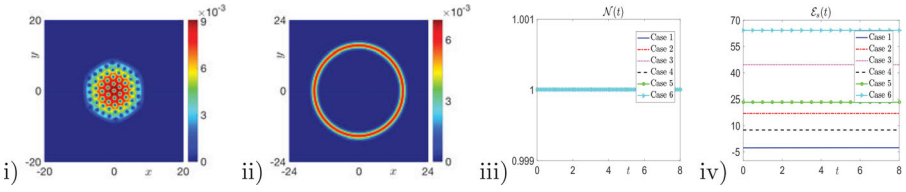

Figure 3. Initial data of *Type 1* (i)) and *Type 2* (ii)) and the evolution of the energy and mass for Cases 1 to 6 in Example 3.2.

Cases 1–3. Choose $\phi_{\rm gs}^{s_0}$ as *Type 1*, let $\mathbf{x}_0 = (0,0)^{\rm T}$, and only change the fractional order in the SFNLSE (8) for the dynamics as $s = 0.8$, $s = 1.2$ and $s = 1.4$, respectively. The other parameters are kept unchanged.

Case 4. Choose $\phi_{\rm gs}^{s_0}$ as *Type 2*, and only shift the initial center of mass, i.e. we set $\mathbf{x}_0 = (5,5)^{\rm T}$. The other parameters are kept unchanged.

Case 5. Choose $\phi_{\rm gs}^{s_0}$ as *Type 2* and set $\mathbf{x}_0 = (0,0)^{\rm T}$. We perturb the trapping frequency in the y-direction, i.e. we set $\gamma_y = 1.3$. The other parameters are kept unchanged.

Case 6. Same as *Case 5*, but now perturb the trapping frequency in both x and y-directions, i.e. we set $\gamma_x = \gamma_y = 1.3$.

Figure 3 (iii) and (iv) shows the evolution of the mass $\mathcal{N}(t)$ and the energy $\mathcal{E}_s(t)$, while Figure 4 shows the contour plots of the density $|\psi(\mathbf{x},t)|^2$ at different times for *Cases 1–6*. From these figures and other experiments not shown here for the sake of brevity, we could see that: (1) The masses and total energies are conserved well for all cases; (2) The fractional order s affects the dynamics significantly and qualitatively. For the *Type 1* initial data, when $s < 1$ (subdispersion), the vortex lattice is more condensed (i.e. the compact support of the density is smaller than the initial setup), and rotates with breather-like dynamics. On the other hand, when $s > 1$ (superdispersion), the vortex lattice is less condensed and similarly rotates with breather-like dynamics. The structure of the vortex lattice is destroyed although some symmetric properties of the density are still kept for long-time dynamics (cf. Figure 4 (a)–(c)). Eventually, a chaotic dynamics and even a turbulent behaviour arises for most cases; (2) For *Type 2* initial data, the ring-structure is destroyed if either the initial center of mass is shifted or the trapping potential are perturbed asymmetrically (cf. Figure 4 (d) and (e)). On the contrary, if only and symmetrically the trapping potential are perturbed, the ring-structure will be kept and the ring undergo a breather-like dynamics (cf. Figure 4 (f)), similar as the dynamics in

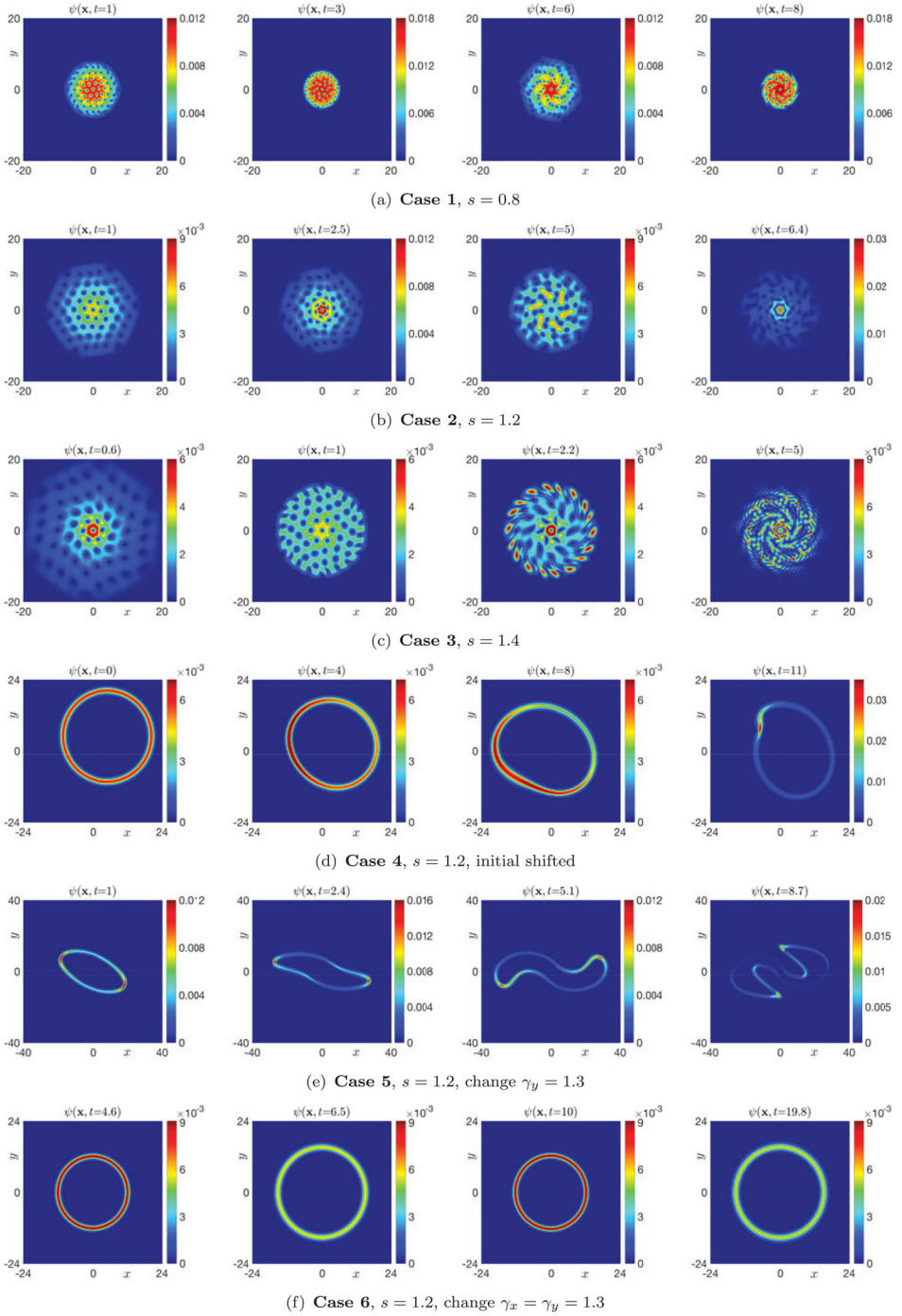

Figure 4. Initial data, contour plots of the density $|\psi(\mathbf{x}, t)|^2$ in Example 3.2. (a) *Case 1*, $s = 0.8$, (b) *Case 2*, $s = 1.2$, (c) *Case 3*, $s = 1.4$, (d) *Case 4*, $s = 1.2$, initial shifted, (e) *Case 5*, $s = 1.2$, change $\gamma_y = 1.3$ and (f) *Case 6*, $s = 1.2$, change $\gamma_x = \gamma_y = 1.3$.

standard NLSE (i.e. $s = 1$). Based on all these examples, we conclude that the dynamics of a fractional BECs modelled by the SFNLSE can be deeply affected by the fractional power s, depending on the sub- or superdispersion situation.

4. The time FNLSE/FGPE

4.1. Time fractional models and dynamical properties

We consider now the general Time-Fractional NLSE (TFNLSE) given by

$$(\gamma_R + \mathrm{i}\gamma_I)(\mathrm{i}{}_0^C\mathcal{D}_t)^\alpha \psi(t,\mathbf{x}) = -\tfrac{1}{2}\Delta\psi + V(\mathbf{x})\psi + \beta|\psi|^2\psi, \quad \mathbf{x}\in\mathbb{R}^d, \ \ t>0, \tag{20}$$

with initial data $\psi(0,\mathbf{x}) = \psi_0(\mathbf{x})$. The operator ${}_0^C\mathcal{D}_t^\alpha$ denotes the Caputo fractional derivative of order α ($0<\alpha<1$) with respect to t [67] and defined by

$${}_0^C\mathcal{D}_t^\alpha \psi(t,\mathbf{x}) = \frac{1}{\Gamma(1-\alpha)}\int_0^t \frac{1}{(t-u)^\alpha}\frac{\partial\psi(u,\mathbf{x})}{\partial u}\mathrm{d}u, \quad 0<\alpha<1, \tag{21}$$

where $\Gamma(\cdot)$ is the Gamma special function. To define a general setting, we introduce a complex-valued coefficient in front of the fractional derivative, i.e. $(\gamma_R + \mathrm{i}\gamma_I)$, where $\gamma_R > 0$ and $\gamma_I \geq 0$. The reason is to get a unified writing of the various models that can be met in the literature, like the following one introduced in [1]

$$\mathrm{i}({}_0^C\mathcal{D}_t)^\alpha \psi(t,\mathbf{x}) = -\tfrac{1}{2}\Delta\psi + V(\mathbf{x})\psi + \beta|\psi|^2\psi, \tag{22}$$

by choosing $\gamma_R + \mathrm{i}\gamma_I = i^{1-\alpha}$, and seen as a modified version of Naber model's [63]

$$(\mathrm{i}{}_0^C\mathcal{D}_t)^\alpha \psi(t,\mathbf{x}) = -\tfrac{1}{2}\Delta\psi + V(\mathbf{x})\psi + \beta|\psi|^2\psi, \tag{23}$$

corresponding to $\gamma_R = 1$ and $\gamma_I = 0$. Here, we set $({}_0^C\mathcal{D}_t)^\alpha = {}_0^C\mathcal{D}_t^\alpha$. Therefore, one can interpret (22) as an extension of Equation (23) with a dissipative term (up to a multiplicative constant) since indeed $\gamma_R = \cos((1-\alpha)\pi/2) > 0$ and $\gamma_I = \sin((1-\alpha)\pi/2) \geq 0$, for $0<\alpha<1$. This generalizes the standard dissipative form of the GPE [77] which is used in quantum turbulence.

In [30], the authors prove that there is no conservation law for the linear version of (23) (i.e. for $\beta = 0$). In particular, for $0<\alpha<1$, they obtain that

$$\lim_{t\to+\infty} \mathcal{N}(t) = \frac{1}{\alpha^2} > 1, \tag{24}$$

which means that particles are created during the fractional dynamical process (extracted from the confined potential field). In addition, they show that the energy $\mathcal{E}_2(t)$ goes to a limiting value when t tends towards $+\infty$, and is given through averaging. Therefore, since (22) can be seen as a version of Equation (23) with dissipative term, one can expect that inversely a certain amount of particles is absorbed when $\beta = 0$, leading then to a loss of mass and a decay of the energy. To the best of our knowledge, no general result is available for the nonlinear case where probably many possible situations can arise (see Section 4.3 for some numerical illustrations depending on the models and assumptions).

Concerning the dispersion relation, if one uses a travelling plane wave $\psi(t,\mathbf{x}) = A\,\mathrm{e}^{\mathrm{i}(\mathbf{k}\cdot\mathbf{x}-\omega t)}$, and since one gets

$$({}_0^C\mathcal{D}_t)^\alpha(A\,\mathrm{e}^{\mathrm{i}(\mathbf{k}\cdot\mathbf{x}-\omega t)}) = A\,\mathrm{e}^{\mathrm{i}\mathbf{k}\cdot\mathbf{x}}({}_0^C\mathcal{D}_t)^\alpha(\mathrm{e}^{-\mathrm{i}\omega t})$$

and

$$({}_0^C\mathcal{D}_t)^\alpha(\mathrm{e}^{-\mathrm{i}\omega t}) := -\mathrm{i}\omega t^{1-\alpha}E_{1,2-\alpha}(-\mathrm{i}\omega t),$$

where $E_{a,b}$ is the two-parameter Mittag–Leffler special function [35] with parameters $(a,b) := (1, 2-\alpha)$, then the dispersion relation writes

$$-(\gamma_R + \mathrm{i}\gamma_I)i^{1+\alpha}\omega t^{1-\alpha}E_{1,2-\alpha}(-\mathrm{i}\omega t)\,\mathrm{e}^{\mathrm{i}\omega t} = \frac{|\mathbf{k}|^2}{2} + \beta|A|^2, \tag{25}$$

which simplifies to the standard dispersion relation for $\alpha = 1$. Equation (25) is time-dependent and not easy to understand at first sight. Let us nevertheless remark that one gets the asymptotic formula

for the Mittag–Leffler functions

$$E_{a,b}(z) = \frac{1}{a} z^{(1-b)/a}\, \mathrm{e}^{z^{1/a}} - \sum_{r=1}^{N^*} \frac{1}{\Gamma(b-ar)} \frac{1}{z^r} + \mathcal{O}\left(\frac{1}{z^{N^*+1}}\right), \quad \text{for} |\mathrm{z}| \to \infty, |\arg \mathrm{z}| \leq \mu,$$

where $\pi/2 < \mu < \pi$ and $N^* \in \mathbb{N}^*$ and $N^* > 1$. In our situation, $a = 1$, $b = 2 - \alpha$ and $z := -\mathrm{i}\omega t$, which means that $|\arg z| = \pi/2$. As a consequence, we obtain the following asymptotic dispersion formula:

$$(\gamma_R + \mathrm{i}\gamma_I)\omega^\alpha = \frac{|\mathbf{k}|^2}{2} + \beta |A|^2, \tag{26}$$

which now clearly translates the time fractional behaviour of the equation.

With the substitution $\psi \to \psi\, \mathrm{e}^{-iCt}$ and from the Leibniz rule for Caputo fractional derivatives [67] given as an infinite series expansion, the gauge change property does not hold if $\alpha \neq 1$. In addition, the equation is not *a priori* time reversible, in particular because of the dissipation term that may appear. From the discussion above, we see that the situation still needs to be clarified to understand which physical dynamical laws/properties a good discrete scheme should fulfil to be acceptable. This is probably one interesting point to investigate deeper in the future and that will be discussed in Section 4.3 through numerical simulations. Before that, we introduce in Section 4.2 some discretization schemes as well as their efficient implementation, most particularly regarding the computational cost, memory storage and order of accuracy.

4.2. Numerical schemes and their efficient implementation

As in the previous sections, we assume that we can restrict the computational domain to a finite box $\mathcal{D} :=]a; b[$ with suitable boundary conditions (homogeneous Dirichlet/Neumann or periodic boundary conditions).

Before developing some discretization schemes for the full fractional system (20), we first address the problem of designing fast evaluation schemes for the fractional Caputo derivative. This operator depends on the history information and various discretization schemes can be developed, such as the L1-approximation [46,50,56,72] given at time t_n by

$${}^{\mathrm{G}}_{0}\mathbb{D}^{\alpha}_{t_n}\psi^n = \frac{\Delta t^{-\alpha}}{\Gamma(2-\alpha)} \sum_{k=1}^{n} a_{n-k}(\psi^k - \psi^{k-1}), \tag{27}$$

where $a_k = (k+1)^{1-\alpha} - k^{1-\alpha}$ $(k \geq 0)$. If $\psi \in \mathcal{C}^2([0,T])$, the truncation error satisfies [56,72]

$$|{}^{\mathrm{C}}_{0}\mathcal{D}^{\alpha}_{t_n}\psi^n - {}^{\mathrm{G}}_{0}\mathbb{D}^{\alpha}_{t_n}\psi^n| \leq C\Delta t^{2-\alpha}. \tag{28}$$

A high-order scheme for the Caputo derivative is the L2-1_σ formula proposed in [2]. The scheme is approximated at the time point $t_{n+\sigma}$, with $\sigma = 1 - \alpha/2$, by

$${}^{H}\mathbb{D}^{\alpha}_{t}\psi^{n+\sigma} = \frac{1}{\Gamma(1-\alpha)} \left(\sum_{k=1}^{n} \int_{t_{k-1}}^{t_k} \frac{(\Pi_{2,k}\psi(s))'}{(t_{n+\sigma}-s)^\alpha} \mathrm{d}s + \int_{t_n}^{t_{n+\sigma}} \frac{(\Pi_{1,n}\psi(s))'}{(t_{n+\sigma}-s)^\alpha} \mathrm{d}s \right), \tag{29}$$

where $\Pi_{2,n}\psi(t)$ and $\Pi_{1,n}\psi(t)$ are the quadratic and linear interpolations given by

$$\Pi_{2,n}\psi(t) = \psi^{n-1}\frac{(t-t_n)(t-t_{n+1})}{2\Delta t^2} - \psi^{n}\frac{(t-t_{n-1})(t-t_{n+1})}{\Delta t^2} + \psi^{n+1}\frac{(t-t_{n-1})(t-t_n)}{2\Delta t^2},$$

$$\Pi_{1,n}\psi(t) = \psi^{n}\frac{t_{n+1}-t}{\Delta t} + \psi^{n+1}\frac{t-t_n}{\Delta t}.$$

As shown in [2] under the assumption that $\psi \in \mathcal{C}^3([0,T])$, the truncation error satisfies

$$ {}_0^C\mathcal{D}_t^\alpha \psi(t_{n+\sigma}) = {}^H\mathbb{D}_t^\alpha \psi^{n+\sigma} + \mathcal{O}(\Delta t^{3-\alpha}), \quad n = 0, 1, \ldots, N-1. $$

From the approximation (27), one can see that evaluating the Caputo fractional derivative requires the storage of all the discrete past values of the unknown wave function ψ, i.e. $\psi^0, \psi^1, \ldots, \psi^n$, and $\mathcal{O}(n)$ flops at the nth time step and for each spatial grid point x_j, where $j = 0, \ldots, J$. Thus, in the one-dimensional case (i.e. $d=1$), the average storage is $\mathcal{O}(NJ)$ and the total computational cost is $\mathcal{O}(N^2 J)$, which is clearly much larger than for the standard case (see Table 1). As a consequence, this is a severe limitation for the long-time simulation of the TFNLSE, most particularly for higher dimensional problems since the number of grid points then grows as J^d. To reduce both the storage and computational cost, fast evaluation algorithms of the Caputo derivative can be built [39]. The main idea of the acceleration method is to split the Caputo derivative into the sum of a local time part and a history part

$$ \begin{aligned} {}_0^C\mathcal{D}_{t_n}^\alpha \psi &= \frac{1}{\Gamma(1-\alpha)} \int_{t_{n-1}}^{t_n} \frac{\psi'(u,x)}{(t_n-u)^\alpha} \mathrm{d}u + \frac{1}{\Gamma(1-\alpha)} \int_0^{t_{n-1}} \frac{\psi'(u,x)}{(t_n-u)^\alpha} \mathrm{d}u \\ &:= C_{\mathrm{loc}}(t_n,x) + C_{\mathrm{hist}}(t_n,x). \end{aligned} $$

For the local part $C_{\mathrm{loc}}(t_n,x)$, we apply the L1-approximation, i.e.

$$ C_{\mathrm{loc}}(t_n,x) \approx \frac{\psi(t_n,x)-\psi(t_{n-1},x)}{\Gamma(1-\alpha)\Delta t} \int_{t_{n-1}}^{t_n} \frac{1}{(t_n-u)^\alpha} \mathrm{d}u = \frac{\psi(t_n,x)-\psi(t_{n-1},x)}{\Gamma(2-\alpha)\Delta t^\alpha}, \tag{30} $$

while for the history part $C_{\mathrm{hist}}(t_n,x)$, we integrate by part and get

$$ C_{\mathrm{hist}}(t_n,x) = \frac{1}{\Gamma(1-\alpha)} \left[\frac{\psi(t_{n-1},x)}{\Delta t^\alpha} - \frac{\psi(t_0,x)}{t_n^\alpha} - \alpha \int_0^{t_{n-1}} \frac{\psi(u,x)}{(t_n-u)^{1+\alpha}} \mathrm{d}u \right]. \tag{31} $$

The sum-of-exponentials expansion can be used to approximate the kernel $t^{-1-\alpha}$. More precisely, for a given absolute error ε and for α, there exist some positive real numbers s_ℓ and w_ℓ, with $\ell = 1, \ldots, N_{\mathrm{exp}}$ (N_{exp} is the number of exponentials), such that

$$ \left| \frac{1}{t^{1+\alpha}} - \sum_{\ell=1}^{N_{\mathrm{exp}}} \omega_\ell \, \mathrm{e}^{-s_\ell t} \right| \le \varepsilon, \quad \text{for all } t \in [\Delta t, T]. \tag{32} $$

By replacing in Equation (31) the kernel $t^{-1-\alpha}$ by its sum-of-exponentials approximation in Equation (32), we deduce

$$ C_{\mathrm{hist}}(t_n,x) \approx \frac{1}{\Gamma(1-\alpha)} \left[\frac{\psi(t_{n-1},x)}{\Delta t^\alpha} - \frac{\psi(t_0,x)}{t_n^\alpha} - \alpha \sum_{\ell=1}^{N_{\mathrm{exp}}} \omega_\ell U_{\mathrm{hist},\ell}(t_n,x) \right]. $$

The term $U_{\mathrm{hist},\ell}(t_n,x)$ is defined by

$$ U_{\mathrm{hist},\ell}(t_n,x) = \int_0^{t_{n-1}} \mathrm{e}^{-(t_n-u)s_\ell} \psi(u,x) \, \mathrm{d}u, $$

and has a simple recurrence relation

$$ U_{\mathrm{hist},\ell}(t_n,x) = \mathrm{e}^{-s_\ell \Delta t} U_{\mathrm{hist},\ell}(t_{n-1},x) + \int_{t_{n-2}}^{t_{n-1}} \mathrm{e}^{-s_\ell (t_n-u)} \psi(u,x) \, \mathrm{d}u, \tag{33} $$

with $U_{\text{hist},\ell}(t_0,x)=0$. The integral can be calculated by

$$\begin{aligned}&\int_{t_{n-2}}^{t_{n-1}} \mathrm{e}^{-s_\ell(t_n-u)}\psi(u,x)\,\mathrm{d}u\\ &\approx \frac{\mathrm{e}^{-s_\ell\Delta t}}{s_\ell^2\Delta t}\left[(\mathrm{e}^{-s_\ell\Delta t}-1+s_\ell\Delta t)\psi^{n-1}+(1-\mathrm{e}^{-s_\ell\Delta t}-\mathrm{e}^{-s_\ell\Delta t}s_\ell\Delta t)\psi^{n-2}\right].\end{aligned}$$

Finally, the fast approximate evaluation of the Caputo fractional derivative is given by the formula

$$\begin{aligned}{}_0^{FC}\mathbb{D}_{t_n}^{\alpha}\psi^n &= \frac{\psi(t_n,x)-\psi(t_{n-1},x)}{\Gamma(2-\alpha)\Delta t^{\alpha}}\\ &\quad+\frac{1}{\Gamma(1-\alpha)}\left[\frac{\psi(t_{n-1},x)}{\Delta t^{\alpha}}-\frac{\psi(t_0,x)}{t_n^{\alpha}}-\alpha\sum_{\ell=1}^{N_{\text{exp}}}\omega_\ell U_{\text{hist},\ell}(t_n,x)\right],\end{aligned}\tag{34}$$

for $n>0$, and where $U_{\text{hist},\ell}(t_n,x)$ can be obtained by the recurrence relation (33). As shown in [39], if $\psi(t)\in\mathcal{C}^2([0,t_n])$, then the truncated error is

$$|{}_0^{C}\mathcal{D}_{t_n}^{\alpha}\psi-{}_0^{FC}\mathbb{D}_{t_n}^{\alpha}\psi|\le C(\Delta t^{2-\alpha}+\varepsilon).\tag{35}$$

For the fast evaluation of the L2-1$_\sigma$ scheme, we approximate the kernel $(t_{n+\sigma}-s)^{-\alpha}$, for $s\in(0,t_n)$, in Equation (29) and use a linear interpolation $\Pi_{1,n}\psi'(s)$, for $s\in(t_n,t_{n+\sigma})$, yielding

$$\begin{aligned}&{}_0^{C}\mathcal{D}_t^{\alpha}\psi(t_{n+\sigma})\\ &\approx\frac{1}{\Gamma(1-\alpha)}\left(\int_0^{t_n}\psi'(s)\sum_{\ell=1}^{N_{\text{exp}}}w_\ell\,\mathrm{e}^{-s_\ell(t_{n+\sigma}-s)}\,\mathrm{d}s+\int_{t_n}^{t_{n+\sigma}}\frac{(\Pi_{1,n}\psi(s))'}{(t_{n+\sigma}-s)^{\alpha}}\mathrm{d}s\right)\\ &=\sum_{\ell=1}^{N_{\text{exp}}}\frac{w_\ell}{\Gamma(1-\alpha)}\int_0^{t_n}\psi'(s)\,\mathrm{e}^{-s_\ell(t_{n+\sigma}-s)}\,\mathrm{d}s+\frac{1}{\Gamma(1-\alpha)}\frac{(\psi^{n+1}-\psi^n)}{\Delta t}\int_{t_n}^{t_{n+\sigma}}\frac{1}{(t_{n+\sigma}-s)^{\alpha}}\mathrm{d}s\\ &=\sum_{\ell=1}^{N_{\text{exp}}}\frac{1}{\Gamma(1-\alpha)}w_\ell V_\ell^n+\lambda a_0(\psi^{n+1}-\psi^n),\end{aligned}$$

where

$$\lambda=\frac{\Delta t^{-\alpha}}{\Gamma(2-\alpha)},\quad a_0=\sigma^{1-\alpha},\quad V_\ell^n=\int_0^{t_n}\psi'(s)\,\mathrm{e}^{-s_\ell(t_{n+\sigma}-s)}\,\mathrm{d}s.$$

The history part V_ℓ^n can be calculated by using a recursive relation and a quadratic interpolation, namely

$$\begin{aligned}V_\ell^n&=\int_0^{t_n}\psi'(s)\,\mathrm{e}^{-s_\ell(t_{n+\sigma}-s)}\,\mathrm{d}s\\ &\approx\int_{t_0}^{t_{n-1}}\psi'(s)\,\mathrm{e}^{-s_\ell(t_{n+\sigma}-s)}\,\mathrm{d}s+\int_{t_{n-1}}^{t_n}(\Pi_{2,n}\psi(t))'\,\mathrm{e}^{-s_\ell(t_{n+\sigma}-s)}\,\mathrm{d}s\\ &=\mathrm{e}^{-s_\ell\Delta t}V_\ell^{n-1}+A_\ell(\psi^n-\psi^{n-1})+B_\ell(\psi^{n+1}-\psi^n),\end{aligned}\tag{36}$$

where

$$A_\ell=\int_0^1(3/2-s)\,\mathrm{e}^{-s_\ell\Delta t(\sigma+1-s)}\,\mathrm{d}s,\quad B_\ell=\int_0^1(s-1/2)\,\mathrm{e}^{-s_\ell\Delta t(\sigma+1-s)}\,\mathrm{d}s.$$

Overall, the FL2-1$_\sigma$ formula for ${}_0^C\mathcal{D}_t^\alpha$ proposed in [82] is given by

$$ {}^{HH}\mathbb{D}_t^\alpha \psi^{n+\sigma} = \sum_{\ell=1}^{N_{\rm exp}} \frac{1}{\Gamma(1-\alpha)} w_\ell V_\ell^n + \lambda a_0(\psi^{n+1} - \psi^n), \tag{37}$$

where, if $\psi(t) \in \mathcal{C}^3([0,T])$, an error estimate is

$$ |{}_0^C\mathcal{D}_{t_n}^\alpha \psi - {}_0^{FH}\mathbb{D}_{t_n}^\alpha \psi| \le C(\Delta t^{3-\alpha} + \varepsilon). \tag{38}$$

Meanwhile, the number of exponentials $N_{\rm exp}$ is estimated [39] by

$$ N_{\rm exp} = \mathcal{O}\left(\log\frac{1}{\varepsilon}\left(\log\log\frac{1}{\varepsilon} + \log\frac{T}{\Delta t}\right) + \log\frac{1}{\Delta t}\left(\log\log\frac{1}{\varepsilon} + \log\frac{1}{\Delta t}\right)\right).$$

For a fixed accuracy ε, we have $N_{\rm exp} = \mathcal{O}(\log N)$ for $T \gg 1$ or $N_{\rm exp} = \mathcal{O}(\log^2 N)$ for $T \approx 1$, where $N = T/\Delta t$. The resulting algorithm has a nearly optimal complexity, requiring $\mathcal{O}(NJN_{\rm exp})$ operations and a $\mathcal{O}(JN_{\rm exp})$ storage for solving the TFNLSE. We remark that a linear system must be solved at each time step, therefore at the same cost as for the standard case $\alpha = 1$. Other efforts to speed-up the evaluation of weakly singular kernels can be found in [3,41,58,60,84].

Thus, we apply the L1 scheme to approximate the time-fractional Caputo derivative, the second-order central finite-difference method to approximate the second-order spatial derivative ∂_{xx} by Δ_h, and use a linearized scheme to approximate the nonlinear term. We respectively have the direct scheme

$$ (\gamma_R + \mathrm{i}\gamma_I)(i_0^C\mathbb{D}_{t_n})^\alpha \psi_j^n = -\tfrac{1}{2}\Delta_h \psi_j^n + \left[V_j + \beta|\psi_j^{n-1}|^2\right]\psi_j^n, \tag{39}$$

and the corresponding fast scheme

$$ (\gamma_R + \mathrm{i}\gamma_I)(i_0^{FC}\mathbb{D}_{t_n})^\alpha \psi_j^n = -\tfrac{1}{2}\Delta_h \psi_j^n + \left[V_j + \beta|\psi_j^{n-1}|^2\right]\psi_j^n, \tag{40}$$

for $1 \le j \le J-1$. As discussed in [83], the convergence orders of the schemes (39) and (40) are respectively $\mathcal{O}(h^2 + \Delta t)$ and $\mathcal{O}(h^2 + \Delta t + \varepsilon)$, if the solution ψ is smooth enough. We point out that the choice of ε is far smaller than $(h^2 + \Delta t)$ to not affect the convergence order. In addition, FFT-based SP schemes can also be easily adapted from Sections 2 and 3. Another possible scheme is to use the relaxation technique introduced by Li *et al.* in [52] for the direct method

$$ (\gamma_R + \mathrm{i}\gamma_I)(i_0^C\mathbb{D}_{t_n})^\alpha \psi_j^n = -\tfrac{1}{2}\Delta_h \psi_j^n + \left[V_j + \beta|\tilde{\psi}_j^n|^2\right]\psi_j^n, \tag{41}$$

and the fast scheme

$$ (\gamma_R + \mathrm{i}\gamma_I)(i_0^{FC}\mathbb{D}_{t_n})^\alpha \psi_j^n = -\tfrac{1}{2}\Delta_h \psi_j^n + \left[V_j + \beta|\tilde{\psi}_j^n|^2\right]\psi_j^n, \tag{42}$$

with $\tilde{\psi}_j^n = 2\psi_j^{n-1} - \psi_j^{n-2}$. For a smooth enough solution, the truncated errors for the schemes (41) and (42) are, respectively, $\mathcal{O}(h^2 + \Delta t^{2-\alpha})$ and $\mathcal{O}(h^2 + \Delta t^{2-\alpha} + \varepsilon)$. The proof of the convergence above requires to state a nontrivial discretized fractional Gronwall inequality [51].

We now consider the high-order scheme for the TFNLSE, written at time $t_{n+\sigma}$, $n = 0, 1, 2\cdots$, and for any $\psi(t) \in \mathcal{C}^2([0,t_N])$, based on the approximation

$$ \psi(t_{n+\sigma}) = \sigma\psi^{n+1} + (1-\sigma)\psi^n + \mathcal{O}(\Delta t^2), \quad n = 0, 1, \ldots, N-1.$$

The time-fractional Caputo derivative is approximated by the FL2-1$_\sigma$ formula and we adapt the ReFD method for the nonlinear interaction term. The TFNLSE equation is then approximated

at $(t_{n+\sigma}, x_j)$ by

$$
\begin{aligned}
&(1-\sigma)u_j^{n+\sigma} + \sigma u_j^{n-1+\sigma} = \beta|\psi_j^n|^2,\\
&(\gamma_R + \mathrm{i}\gamma_I)({}_0^{FC}\mathbb{D}_{t_n})^{\alpha}\psi_j^{n+\sigma}\\
&\quad = -\tfrac{1}{2}(\sigma\Delta_h\psi_j^{n+1} + (1-\sigma)\Delta_h\psi_j^n) + (V_j + u_j^{n+\sigma})(\sigma\psi_j^{n+1} + (1-\sigma)\psi_j^n).
\end{aligned}
\tag{43}
$$

For a smooth enough solution, the truncated error for Equation (43) is $\mathcal{O}(h^2 + \Delta t^2 + \varepsilon)$, fixing $\sigma = 1 - \alpha/2$.

Let us remark that time-splitting schemes are currently being developed for fractional PDEs [27]. This is probably an interesting future direction to investigate for designing fast TSSP for the TFNLSE, similarly to the schemes presented in Sections 2 and 3. We finally point out that for fractional subdiffusion problems, an essential feature is that the solution always lacks some smoothness near the initial time although it would be smooth away from $t = 0$ (see, e.g. the discussions in [26,40,62,68,70]). The expected order of convergence in time [55] needs the use of nonuniform mesh in the temporal direction, such as a graded mesh $t_n = T(n\Delta t)^{\gamma}$, for a well-chosen value of the parameter $\gamma > 0$.

4.3. Numerical examples

Example 4.1: For our first 1d example, we consider the quadratic potential $V(x) := x^2/2$ and a purely linear TFNLSE, i.e. $\beta := 0$. The initial data are taken as the ground state of the standard linear Schrödinger equation with harmonic trap: $\psi_0(x) := \mathrm{e}^{-x^2/2}/\pi^{1/4}$. The corresponding mass is then equal to 1 and the energy level is 1/2. The final time of computation is $T = 100$ (except for $\alpha = 0.25$, where $T = 800$) for the bounded spatial domain $\mathcal{D} :=]-10, 10[$. The discretization parameters are $\Delta t = 10^{-3}$ and $h = 10^{-2}$. We use the fast second-order scheme (43) (for $\varepsilon = 10^{-11}$). Figure 5 (a)–(c) shows the evolution of the density function $|\psi|^2$, its mass $\mathcal{N}$ and energy $\mathcal{E}_2$, for $(\gamma_R + \mathrm{i}\gamma_I) = 1$ (no dissipation case) and three values of the fractional power, i.e. $\alpha = 0.25, 0.5, 0.75$. We observe that the Gaussian solution is modified according to α, the limit of the mass $\mathcal{N}$ being indeed α^{-2} as predicted by formula (24), and $\lim_{t\to+\infty}\mathcal{E}_2(t) = \alpha^{-2}/2$ from the numerical simulations. An approximation of the limit value of the mass can be obtained through an average over $[0; T]$ of the numerical masses, yielding the estimates 16.93, 4.04, 1.78 approximating the theoretical limits 16.38,4.04,1.78 for $\alpha = 0.25, 0.5, 0.75$, respectively. We observe that the solution fluctuates according to t, gaining/loosing some mass alternatively. The solution also disperses slightly more as α goes to zero (this is more clearly seen in Example 4.2). A formal way to understand this property is by considering the dispersive relation (26) which can also be rewritten and expanded for large spatial frequencies $|\mathbf{k}|$ as follows:

$$
\omega = \frac{|\mathbf{k}|^{2/\alpha}}{(2(\gamma_R + \mathrm{i}\gamma_I))^{1/\alpha}}\left(1 + \frac{2\beta}{|\mathbf{k}|^2}|A|^2\right)^{1/\alpha} \sim \frac{|\mathbf{k}|^{2/\alpha}}{(2(\gamma_R + \mathrm{i}\gamma_I))^{1/\alpha}}\left(1 + \frac{2\beta}{\alpha|\mathbf{k}|^2}|A|^2\right). \tag{44}
$$

Therefore, we can roughly interpret α as s^{-1} in Equation (11) up to a multiplicative constant (that may also be complex-valued). Then, superdispersion formally corresponds to $\alpha < 1$ and subdispersion to $\alpha > 1$. Nevertheless, the situation here shows that the modelling is more complex since a fractional Laplacian also affects the nonlinearity, the corresponding operator acting as a fractional derivative operator for $\alpha < 1$ and a regularizing integral operator for $\alpha > 1$. For longer times, the solution tends to a stationary state for the TFNLSE at fixed α which is expected to be the ground state. To end this first example, we compute on Figure 5(d) the same problem for $\alpha = 0.5$ but with: $(\gamma_R + \mathrm{i}\gamma_I) = i^{1-\alpha}$, which means that we add some dissipation to the model. Therefore, after a sufficiently long time the solution converges to zero as it can be directly observed.

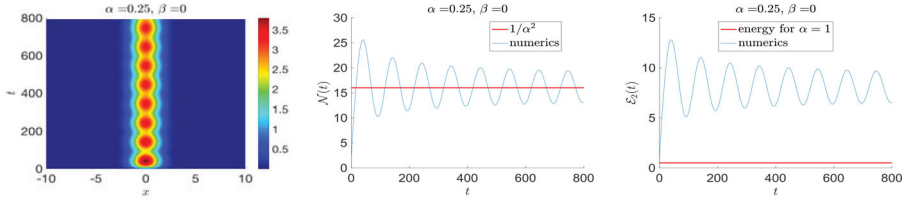

(a) Example 4.1 : $(\gamma_R + i\gamma_I) = 1$, $\alpha = 0.25$, $\beta = 0$

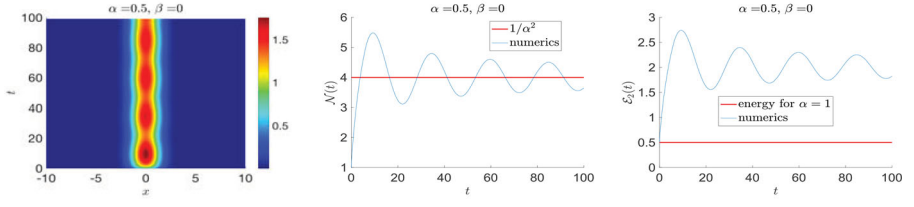

(b) Example 4.1 : $(\gamma_R + i\gamma_I) = 1$, $\alpha = 0.5$, $\beta = 0$

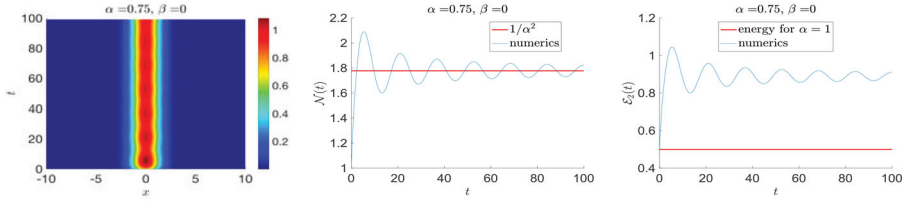

(c) Example 4.1 : $(\gamma_R + i\gamma_I) = 1$, $\alpha = 0.75$, $\beta = 0$

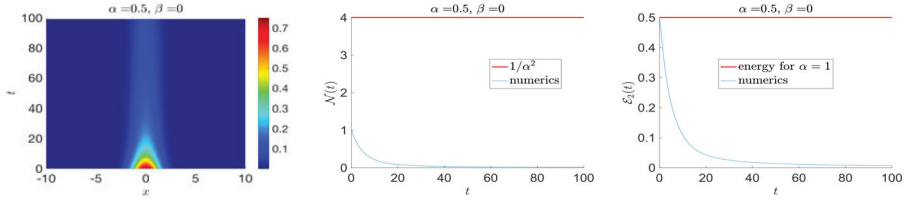

(d) Example 4.1 : $(\gamma_R + i\gamma_I) = i^{1-\alpha}$, $\alpha = 0.5$, $\beta = 0$

Figure 5. Evolution of the density $|\psi(x,t)|^2$, mass $\mathcal{N}(t)$ and energy $\mathcal{E}_2(t)$ for the fractional powers $\alpha = 0.25, 0.5$ and 0.75, and for the linear case $\beta = 0$ for Example 4.1. (a) Example 4.1: $(\gamma_R + \mathrm{i}\gamma_I) = 1, \alpha = 0.25, \beta = 0$, (b) Example 4.1: $(\gamma_R + \mathrm{i}\gamma_I) = 1, \alpha = 0.5, \beta = 0$, (c) Example 4.1: $(\gamma_R + \mathrm{i}\gamma_I) = 1, \alpha = 0.75, \beta = 0$ and (d) Example 4.1: $(\gamma_R + \mathrm{i}\gamma_I) = i^{1-\alpha}, \alpha = 0.5, \beta = 0$.

Example 4.2: For this second example, we consider the TFNLSE with a quadratic potential $V(x) = x^2/2$, and first with a focusing cubic nonlinearity $\beta < 0$. The initial data are given by

$$\psi_0(x) := \frac{A}{\sqrt{-\beta}} \mathrm{sech}(A(x - x_0))\, \mathrm{e}^{\mathrm{i}(\nu x + \theta_0)}, \quad x \in \mathcal{D},$$

with $A = 2$, $x_0 = \nu = \theta_0 = 0$. In the standard situation $\alpha = 1$, and without potential term i.e. $V = 0$, then the mass and energy can be computed analytically [7] as follows:

$$\mathcal{N}(t) := \frac{A}{\sqrt{-\beta}}, \quad \mathcal{E}_2(t) := \frac{A\nu^2}{\beta} + \frac{A^3}{3\beta}, \tag{45}$$

the solution being a soliton. The final time of computation is set to $T = 20$ and the computational domain to $]-10; 10[$. The discretization parameters are $\Delta t := 10^{-3}$ and $h = 5 \times 10^{-3}$.

We start by fixing $(\gamma_R + \mathrm{i}\gamma_I) = 1$ for $\alpha = 0.5$ and 0.75 in Figure 6 (a,b), respectively, for $\beta = -1$. As already noticed above, the superdispersion effect is visible for smaller values of α and some decoherence effect in the wave field seems to appear. In the case of superdispersion, then there is no longer

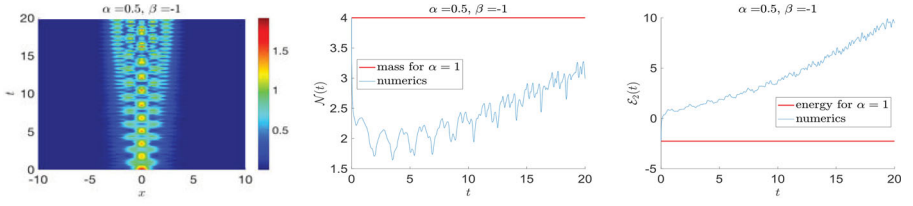

(a) Example 4.2 : $(\gamma_R + i\gamma_I) = 1$, $\alpha = 0.5$, $\beta = -1$

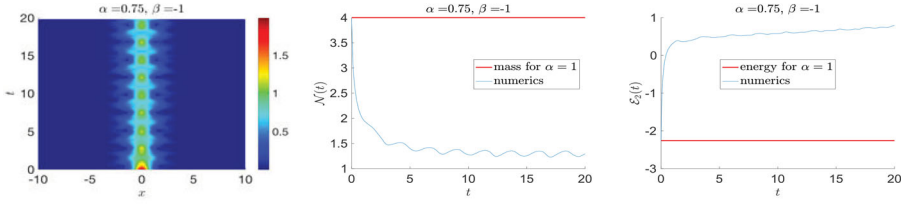

(b) Example 4.2 : $(\gamma_R + i\gamma_I) = 1$, $\alpha = 0.75$, $\beta = -1$

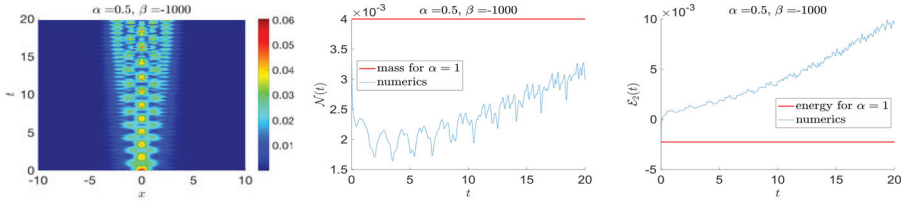

(c) Example 4.2 : $(\gamma_R + i\gamma_I) = 1$, $\alpha = 0.5$, $\beta = -1000$

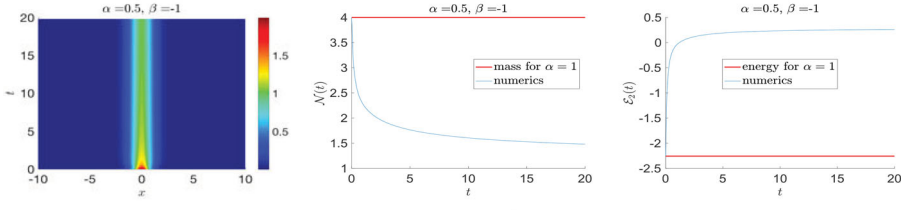

(d) Example 4.2 : $(\gamma_R + i\gamma_I) = i^{1-\alpha}$, $\alpha = 0.5$, $\beta = -1$

Figure 6. Evolution of the density $|\psi(x,t)|^2$, mass $\mathcal{N}(t)$ and energy $\mathcal{E}_2(t)$ for the fractional powers $\alpha = 0.5$ and 0.75 for Example 4.2 (focusing nonlinearity). (a) Example 4.2: $(\gamma_R + \mathrm{i}\gamma_I) = 1$, $\alpha = 0.5$, $\beta = -1$, (b) Example 4.2: $(\gamma_R + \mathrm{i}\gamma_I) = 1$, $\alpha = 0.75$, $\beta = -1$, (c) Example 4.2: $(\gamma_R + \mathrm{i}\gamma_I) = 1, \alpha = 0.5, \beta = -1000$ and (d) Example 4.2: $(\gamma_R + \mathrm{i}\gamma_I) = i^{1-\alpha}, \alpha = 0.5, \beta = -1$.

a compensation between the Laplacian and the nonlinear term as for the standard case, the fractional time derivative introducing some dominant dispersion thanks to Equation (44). Furthermore, the energy globally grows with the time to pass from negative to positive values, $\mathcal{E}_2$ being larger for a given fractional order than for the integer-order case. The energy increases as α gets smaller. The behavior of the mass is difficult to predict, but the value is always smaller than for the standard case. Comparing Figure 6(a,c), we see that the curves for the solutions are exactly the same, up to the scaling factor between the two values of β, which is also consistent with formulae (45) for the standard case (but with a time-dependency for the fractional situation). Figure 6(d) finally reports the case where $(\gamma_R + \mathrm{i}\gamma_I) = i^{1-\alpha}$ for $\alpha = 0.5$ and $\beta = -1$. Compared with Figure 6(a), we clearly observe the effect of the dissipation term even if the solution is actually not zero for longer times, probably because of the nonlinear interactions.

To complete the simulations, we consider now a defocusing nonlinearity $\beta = 1$ in Figure 7 (a)–(c) for $\alpha = 0.5, 0.75$ and $(\gamma_R + \mathrm{i}\gamma_I) = 1$ and $i^{1-\alpha}$. The simulation parameters are the same as previously, but the computational domain is $]-15; 15[$. The behaviour of the solution shows again some superdispersion effects, the evolution of the mass and energy being difficult to describe at the first

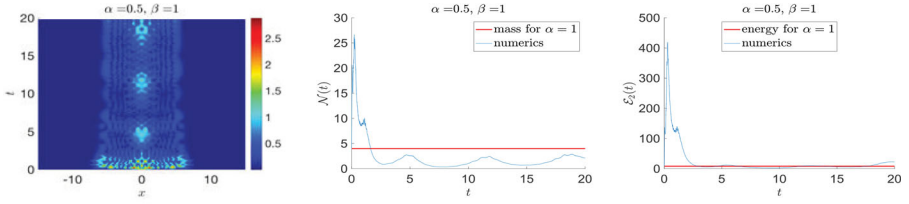

(a) Example 4.2, $(\gamma_R + i\gamma_I) = 1$, $\alpha = 0.5$, $\beta = 1$

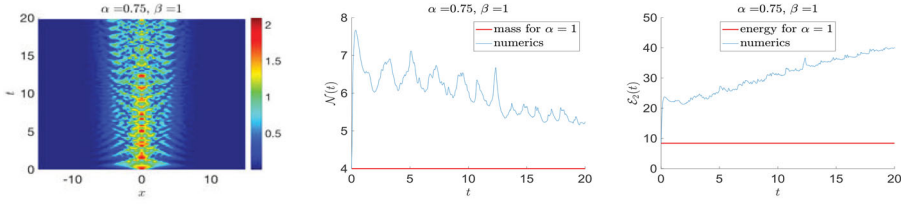

(b) Example 4.2, $(\gamma_R + i\gamma_I) = 1$, $\alpha = 0.75$, $\beta = 1$

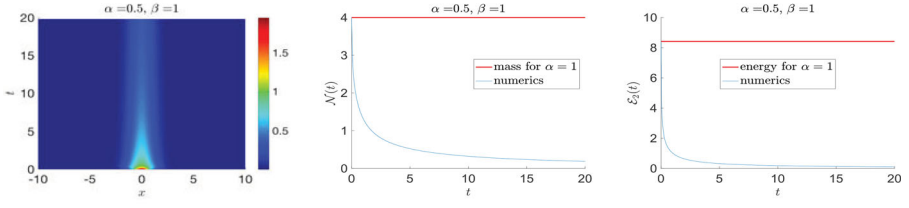

(c) Example 4.2, $(\gamma_R + i\gamma_I) = i^{1-\alpha}$, $\alpha = 0.75$, $\beta = 1$

Figure 7. Evolution of the density $|\psi(x,t)|^2$, mass $\mathcal{N}(t)$ and energy $\mathcal{E}_2(t)$ for the fractional powers $\alpha = 0.5$ and 0.75 for Example 4.2 (defocusing nonlinearity). (a) Example 4.2, $(\gamma_R + \mathrm{i}\gamma_I) = 1, \alpha = 0.5, \beta = 1$, (b) Example 4.2, $(\gamma_R + \mathrm{i}\gamma_I) = 1, \alpha = 0.75, \beta = 1$ and (c) Example 4.2, $(\gamma_R + \mathrm{i}\gamma_I) = i^{1-\alpha}, \alpha = 0.75, \beta = 1$.

sight. When a dissipation term is active (see Figure 7(c)), then we see that the solution tends to zero for large enough times t (the computational domain is $]-10;10[$ here).

5. Conclusion and perspectives

We proposed a few numerical methods for time or space fractional nonlinear Schrödinger equations with some applications in Bose–Einstein condensation. In particular, we focused on the physical properties that a scheme should fulfil at the discrete level. Numerical simulations illustrate the purpose of the paper, trying to highlight some issues for the time fractional case. Building accurate, efficient and stable schemes for the FNLSE remains new and open a lot of future important directions to investigate. Among them, let us mention the extension of some schemes to the FNLSE with time and space varying fractional powers [25], the simulation of coupled systems of FNLSE which can also integrate some nonlocal integral interactions like dipolar or Coulomb potentials, the development of 3d parallel solvers. Finally, one important point which still needs to be deeply understood concerns the link between the physics and the fractional quantum models, most particularly for modelling BECs.

Disclosure statement

No potential conflict of interest was reported by the authors.

Funding

Xavier Antoine thanks the support from the LIASFMA (University of Lorraine), Agence Nationale de la Recherche (grant no. ANR-12-MONU-0007-02 BECASIM) and the hosting of the Beijing CSRC. Qinglin Tang thanks the support

from the Zheng Ge Ru Foundation and the Singapore Ministry of Education Academic Research Fund Tier 2 (grant no. R-146-000-223-112). Jiwei Zhang gratefully acknowledges the support of National Natural Science Foundation of China (grant nos. 91430216 and U1530401).

ORCID


Xavier Antoine http://orcid.org/0000-0002-6501-7757

References

[1] B.N. Achar, B.T. Yale, and J.W. Hanneken, *Time fractional Schrödinger equation revisited*, Adv. Math. Phys. 2013 (2013), Article 290216.
[2] A.A. Alikhanov, *A new difference scheme for the time fractional diffusion equation*, J. Comput. Phys. 280 (2015), pp. 424–438.
[3] B. Alpert, L. Greengard, and T. Hagstrom, *Rapid evaluation of nonreflecting boundary kernels for time-domain wave propagation*, SIAM J. Numer. Anal. 37 (2000), pp. 1138–1164.
[4] X. Antoine and R. Duboscq, *Modeling and computation of bose-einstein condensates: Stationary states, nucleation, dynamics, stochasticity*, in *Nonlinear Optical and Atomic Systems: At the Interface of Mathematics and Physics*, Lecture Notes in Mathematics, Vol. 2146, Springer, Switzerland, 2015, pp. 49–145.
[5] X. Antoine and Q. Tang, *Perfectly matched layers and pseudospectral schemes for the dynamics of Gross–Pitaevskii equations with rotating term*, in preparation (2017).
[6] X. Antoine, A. Arnold, C. Besse, M. Ehrhardt, and A. Schädle, *A review of transparent and artificial boundary conditions techniques for linear and nonlinear Schrödinger equations*, Commun. Comput. Phys. 4 (2008), pp. 729–796.
[7] X. Antoine, W. Bao, and C. Besse, *Computational methods for the dynamics of the nonlinear Schrödinger/Gross-Pitaevskii equations*, Comput. Phys. Commun. 184 (2013), pp. 2621–2633.
[8] X. Antoine, C. Besse, and V. Rispoli, *High-Order IMEX-spectral schemes for computing the dynamics of systems of nonlinear Schrödinger/Gross–Pitaevskii equations*, J. Comput. Phys. 327 (2016), pp. 252–269.
[9] X. Antoine, Q. Tang, and Y. Zhang, *On the ground states and dynamics of space fractional nonlinear Schrödinger/Gross-Pitaevskii equations with rotation term and nonlocal nonlinear interactions*, J. Comput. Phys. 325 (2016), pp. 74–97.
[10] X. Antoine, A. Levitt, and Q. Tang, *Efficient spectral computation of the stationary states of rotating Bose-Einstein condensates by the preconditioned nonlinear conjugate gradient method*, J. Comput. Phys. 343 (2017), pp. 92–109.
[11] X. Antoine, E. Lorin, and Q. Tang, *A friendly review of absorbing boundary conditions and perfectly matched layers for classical and relativistic quantum waves equations*, Mol. Phys. 115 (2017), pp. 1861–1879.
[12] W. Bao and Y. Cai, *Mathematical theory and numerical methods for Bose-Einstein condensation*, Kinet. Relat. Mod. 6 (2013), pp. 1–135.
[13] W. Bao and X. Dong, *Numerical methods for computing ground states and dynamics of nonlinear relativistic Hartree equation for boson stars*, J. Comput. Phys. 230 (2011), pp. 5449–5469.
[14] W. Bao and J. Shen, *A fourth-order time-splitting Laguerre–Hermite pseudospectral method for Bose–Einstein condensates*, SIAM J. Sci. Comput. 26 (2005), pp. 2020–2028.
[15] W. Bao, S. Jin, and P.A. Markowich, *On time-splitting spectral approximation for the Schrödinger equation in the semiclassical regime*, J. Comput. Phys. 175 (2002), pp. 487–524.
[16] W. Bao, S. Jin, and P.A. Markowich, *Numerical study of time-splitting spectral discretization of nonlinear Schödinger equations in the semi-classical regimes*, SIAM J. Sci. Comput. 25 (2003), pp. 27–64.
[17] W. Bao, H. Jian, N.J. Mauser, and Y. Zhang, *Dimension reduction of the Schrödinger equation with Coulomb and anisotropic confining potentials*, SIAM J. Appl. Math. 73 (2013), pp. 2100–2123.
[18] W. Bao, Q. Tang, and Z. Xu, *Numerical methods and comparison for computing dark and bright solitons in the nonlinear Schrödinger equation*, J. Comput. Phys. 235 (2013), pp. 423–445.
[19] W. Bao, Q. Tang, and Y. Zhang, *Accurate and efficient numerical methods for computing ground states and dynamics of dipolar Bose-Einstein condensates via the nonuniform FFT*, Commun. Comput. Phys. 19 (2016), pp. 1141–1166.
[20] C. Besse, *A relaxation scheme for nonlinear Schrödinger equation*, SIAM J. Numer. Anal. 42 (2004), pp. 934–952.
[21] C. Besse, B. Bidégaray, and S. Descombes, *Order Estimates in Time of Splitting Methods for the Nonlinear Schrödinger Equation*, SIAM J. Numer. Anal. 40 (2002), pp. 26–40.
[22] C. Besse, G. Dujardin, and I. Lacroix-Violet, *High-order exponential integrators for nonlinear Schrödinger equations with application to rotating Bose-Einstein condensates*, preprint (2015). Available at arXiv:1507.00550v2.
[23] M. Bhatti, *Fractional Schrödinger wave equation and fractional uncertainty principle*, Int. J. Contem. Math. Sci. 2 (2007), pp. 943–950.
[24] A.H. Bhrawy and M.A. Abdelkawy, *A fully spectral collocation approximation for multi-dimensional fractional Schrödinger equations*, J. Comput. Phys. 294 (2015), pp. 462–483.

[25] A.H. Bhrawy and M.A. Zaky, *Highly accurate numerical schemes for multi-dimensional space variable-order fractional Schrödinger equations*, Comput. Math. Appl. 73(6) (2017), pp. 1100–1117.
[26] H. Brunner, L. Ling, and M. Yamamoto, *Numerical simulations of 2D fractional subdiffusion problems*, J. Comput. Phys. 229 (2010), pp. 6613–6622.
[27] W. Cao, Z. Zhang, and G.E. Karniadakis, *Time-splitting schemes for fractional differential equations I: Smooth solutions*, SIAM J. Sci. Comput. 37(4) (2015), pp. A1752–A1776.
[28] I. Carusotto and C. Ciuti, *Quantum fluids of light*, Rev. Mod. Phys. 85 (2013), pp. 299–366.
[29] T. Cazenave, *Semilinear Schrödinger Equations*, Courant Lect. Notes Math., vol. 10, Amer. Math. Soc., Providence RI, 2003.
[30] J. Dong and M. Xu, *Space-time fractional Schrödinger equation with time-independent potentials*, J. Math. Anal. Appl. 344(2) (2008), pp. 1005–1017.
[31] S. Duo and Y. Zhang, *Mass conservative method for solving the fractional nonlinear Schrödinger equation*, Comput. Math. Appl. 71 (2016), pp. 2257–2271.
[32] A. Elgart and B. Schlein, *Mean field dynamics of boson stars*, Comm. Pure Appl. Math. 60 (2007), pp. 500–545.
[33] J. Fröhlich, B.L.G. Jonsson, and E. Lenzmann, *Effective dynamics for boson stars*, Nonlinearity 20 (2007), pp. 1031–1075.
[34] R. Garrappa, I. Moret, and M. Popolizio, *Solving the time-fractional Schrödinger equation by Krylov projection methods*, J. Comput. Phys. 293 (2015), pp. 115–134.
[35] H.J. Haubold, A.M. Mathai, and R.K. Saxena, *Mittag–Leffler functions and their applications*, J. Appl. Math. 2011 (2011), Article 298628.
[36] B. Hicdurmaz and A. Ashyralyev, *A stable numerical method for multidimensional time fractional Schrödinger equation*, Comput. Math. Appl. 72 (2016), pp. 1703–1713.
[37] Z. Huang, S. Jin, P.A. Markowich, and C. Sparber, *A Bloch decomposition based numerical method for quantum dynamics in periodic potentials*, SIAM J. Sci. Comput. 29 (2007), pp. 515–538.
[38] Z. Huang, S. Jin, P.A. Markowich, and C. Sparber, *Numerical simulation of the nonlinear Schrödinger equation with multidimensional periodic potentials*, Mult. Model. Simul. 7 (2008), pp. 539–564.
[39] S. Jiang, J. Zhang, Q. Zhang, and Z. Zhang, *Fast evaluation of the Caputo fractional derivative and its applications to fractional diffusion equations*, Commun. Comput. Phys. to appear, arXiv:1511.03453.
[40] B. Jin, R. Lazarov, and Z. Zhou, *An analysis of the L1 scheme for the subdiffusion equation with nonsmooth data*, IMA J. Numer. Anal. 36(1) (2016), pp. 197–221.
[41] R. Ke, M. Ng, and H. Sun, *A fast direct method for block triangular Toeplitz-like with tri-diagonal block systems from time-fractional partial differential equations*, J. Comput. Phys. 303 (2015), pp. 203–211.
[42] A.Q.M. Khaliq, X. Liang, and K.M. Furati, *A fourth-order implicit-explicit scheme for the space fractional nonlinear Schrödinger equations*, Numer. Algorithms 75(1) (2017), pp. 147–172.
[43] N. Khan, M. Jamil, and A. Ara, *Approximate solutions to time-fractional Schrödinger equation via homotopy analysis method*, ISRN Math. Phys. 2012 (2012), Article 197068.
[44] K. Kirkpatrick and Y. Zhang, *Fractional Schrödinger dynamics and decoherence*, Phys. D 332 (2016), pp. 41–54.
[45] D. Kusnezov, A. Bulgac, and G. Dang, *Quantum Lévy processes and fractional kinetics*, Phys. Rev. Lett. 82 (1999), pp. 1136–1139.
[46] T. Langlands and B. Henry, *The accuracy and stability of an implicit solution method for the fractional diffusion equation*, J. Comput. Phys. 205 (2005), pp. 719–736.
[47] N. Laskin, *Fractional quantum mechanics*, Phys. Rev. E 62 (2000), pp. 3135–3145.
[48] N. Laskin, *Fractional quantum mechanics and Lévy path integrals*, Phys. Lett. A 268 (2000), pp. 298–305.
[49] N. Laskin, *Fractals and quantum mechanics*, Chaos 10 (2000), pp. 780–790.
[50] C. Li, W. Deng, and Y. Wu, *Numerical analysis and physical simulations for the time fractional radial diffusion equation*, Comput. Math. Appl. 62 (2011), pp. 1024–1037.
[51] D. Li, H.-L. Liao, W. Sun, J. Wang, and J. Zhang, *Analysis of L1-Galerkin FEMs for time-fractional nonlinear parabolic problems*, preprint (2016). Available at arXiv:1612.00562v1.
[52] D. Li, J. Wang, and J. Zhang, *Unconditionally convergent L1-Galerkin FEMs for nonlinear time-fractional Schrödinger equations*, preprint (2017).
[53] D. Li, J. Zhang, and Z. Zhang, *The numerical computation of the time-fractional linear Schrödinger equation on unbounded domain*, preprint (2017).
[54] X. Liang, A.Q.M. Khaliq, H. Bhatt, and K.M. Furati, *The locally extrapolated exponential splitting scheme for multi-dimensional nonlinear space-fractional Schrödinger equations*, Numer. Algorithms (2017), pp. 1–20. doi:10.1007/s11075-017-0291-3.
[55] H. Liao, D. Li, J. Zhang, and Y. Zhao, *Sharp error estimate of nonuniform L1 formula for time-fractional reaction-subdiffusion equations*, preprint (2017).
[56] Y. Lin and C. Xu, *Finite difference/spectral approximations for the time-fractional diffusion equation*, J. Comput. Phys. 225 (2007), pp. 1533–1552.
[57] A. Lomin, *Fractional-time quantum dynamics*, Phys. Rev. E 62 (2000), pp. 3135–3145.

[58] X. Lu, H. Sun, and H. Pang, *Fast approximate inversion of a block triangular Toeplitz matrix with applications to fractional sub-diffusion equations*, Numer. Linear Algebra Appl. 22 (2015), pp. 866–882.
[59] C. Lubich, *On splitting methods for Schrödinger-Poisson and cubic nonlinear Schrödinger equations*, Math. Comp. 77 (2008), pp. 2141–2153.
[60] C. Lubich and A. Schädle, *Fast convolution for nonreflecting boundary conditions*, SIAM J. Sci. Comput. 24 (2002), pp. 161–182.
[61] A. Mohebbi, M. Abbaszadeh, and M. Dehghan, *The use of a meshless technique based on collocation and radial basis functions for solving the time fractional nonlinear Schrödinger equation arising in quantum mechanics*, Eng. Anal. Bound Elem. 37 (2013), pp. 475–485.
[62] K. Mustapha, *An implicit finite-difference time-stepping method for a sub-diffusion equation, with spatial discretization by finite elements*, IMA J. Numer. Anal. 31 (2011), pp. 719–739.
[63] M. Naber, *Time fractional Schrödinger equation*, J. Math. Phys. 45 (2004), pp. 3339–3352.
[64] Z. Odibat, S. Momani, and A. Alawneh, *Analytic study on time-fractional Schrödinger equations: Exact solutions by GDTM*, J. Phys. 96 (2008), Article 012066.
[65] F. Pinsker, W. Bao, Y. Zhang, H. Ohadi, A. Dreismann, and J.J. Baumberg, *Fractional quantum mechanics in polariton condensates with velocity-dependent mass*, Phys. Rev. B 92 (2015), Article 195310.
[66] L.P. Pitaevskii and S. Stringari, *Bose-Einstein Condensation*, Clarendon Press, Oxford, 2003.
[67] I. Podlubny, *Fractional Differential Equations*, Academic Press, San Diego, CA, 1999.
[68] K. Sakamoto and M. Yamamoto, *Initial value/boundary value problems for fractional diffusion-wave equations and applications to some inverse problems*, J. Math. Anal. Appl. 382 (2011), pp. 426–447.
[69] J. Shen, T. Tang, and L.-L. Wang, *Spectral Methods. Algorithms, Analysis and Applications*, Springer, Berlin, 2011.
[70] M. Stynes, E. O'Riordan, and J.L. Gracia, *Error analysis of a finite difference method on graded meshes for a time-fractional diffusion equation*, SIAM J. Numer. Anal. 55 (2017), pp. 1057–1079.
[71] C. Sulem and P. Sulem, *The Nonlinear Schrödinger Equation: Self-Focusing and Wave Collapse*, Springer, New York, 1999.
[72] Z. Sun and X. Wu, *A fully discrete difference scheme for a diffusion-wave system*, Appl. Numer. Math. 56 (2006), pp. 193–209.
[73] V.E. Tarasov, *Fractional Heisenberg equation*, Phys. Lett. A 372 (2006), pp. 2984–2988.
[74] M. Thalhammer, *High-order exponential operator splitting methods for time-dependent Schrödinger equations*, SIAM J. Numer. Anal. 46 (2008), pp. 2022–2038.
[75] M. Thalhammer, *Convergence analysis of high-order time-splitting pseudo-spectral methods for nonlinear Schrödinger equations*, SIAM J. Numer. Anal. 50 (2012), pp. 3231–3258.
[76] M. Thalhammer and J. Abhau, *A numerical study of adaptive space and time discretisations for Gross–Pitaevskii equations*, J. Comput. Phys. 231 (2012), pp. 6665–6681.
[77] M. Tsubota, K. Kasamatsu, and M. Ueda, *Vortex lattice formation in a rotating Bose–Einstein condensate*, Phys. Rev. A 65 (2002), p. 023603.
[78] S. Wang and M. Xu, *Generalized fractional Schrödinger equation with space-time fractional derivatives*, J. Math. Phys. 48(4) (2007), p. 043502.
[79] L. Wei, Y. He, X. Zhang, and S. Wang, *Analysis of an implicit fully discrete local discontinuous Galerkin method for the time-fractional Schrödinger equation*, Finite Elem. Anal. Des. 59 (2012), pp. 28–34.
[80] B.J. West, *Quantum Lévy propagators*, J. Phys. Chem. B 104 (2000), pp. 3830–3832.
[81] B. West, M. Bologna, and P. Grigolini, *Physics of Fractal Operators*, Springer, New York, 2002.
[82] Y. Yan, Z. Sun, and J. Zhang, *Fast evaluation of the Caputo fractional derivative and its applications to fractional diffusion equations: a second-order scheme*, Comput. Commun. Phys. 22 (2017), pp. 1028–1048.
[83] J. Zhang, D. Li, and X. Antoine, *Efficient numerical computation of time-fractional nonlinear Schrödinger equations in unbounded domain*, Commun. Comput. Phys. (2018), to appear.
[84] C. Zheng, *Approximation, stability and fast evaluation of exact artificial boundary condition for one-dimensional heat equation*, J. Comput. Math. 25 (2007), pp. 730–745.
[85] C. Zheng, *A perfectly matched layer approach to the nonlinear Schrödinger wave equation*, J. Comput. Phys. 227 (2007), pp. 537–556.